Light Metals 2013 *Edited by: Barry Sadler*
TMS (The Minerals, Metals & Materials Society), 2013

MHD OF ALUMINIUM CELLS WITH THE EFFECT OF CHANNELS AND CATHODE PERTURBATION ELEMENTS

Valdis Bojarevics
University of Greenwich, Park Row, London, SE10 9LS, UK

Keywords: aluminium reduction cells, magnetohydrodynamics, wave instability

Abstract

The industry oriented MHD software for aluminium electrolysis cells is updated to take into account the variation of bottom and top surfaces of the cell cavity. The extended model capabilities include the presence of connected channels, height non-uniformities of the cell bottom affecting the liquid metal hydrodynamics and the electric current passage to the cathode with ridges and variable bottom ledge. The numerical results for 500 kA test cell are used to analyze the cell stability under combination of the effects. Perturbations created by the horizontal current density above the carbon elevations lead to the metal/electrolyte interface wave growth, which is opposed by the increased turbulent damping over the bottom with ridges. Optimization of the cell design permits to improve the cell stability and efficiency.

1. Introduction

The electrolyte channels between and under the anodes, where the gas escapes, are demonstrated to have a crucial effect determining the shape and size of the metal-bath interface deformation [1, 2]. With the electrolyte channels the interface deformation in the stationary case increases significantly. The models used for unsteady wave or stability problems are typically restricted to the mathematical developments not accounting for the channels, see for example [3, 4]. Recently a theory and numerical model of the electrolysis cell was extended to the cases of variable bottom of aluminium layer, the variable thickness of the electrolyte due to the anode non-uniform burn process and the presence of the side channels [5]. However, the free surface in the electrolyte channels was not accounted for in the theoretical development, effectively assuming that the rigid lid surface condition is imposed at the anode bottom and the channels. In this paper we extend the theory of unsteady wave development in the presence of connected channels with the free surface and investigate the effects of the cathode bottom non-uniformities [6-8].

2. The setup for the mathematical model

It is important to have a view to an integrated picture of the whole aluminium cell arrangement in the pot line. The MHD model for a cell in a pot line is shown in Figure 1 for a particular case of the cell location at the end of the line. Most of the cells are in the mid position between the neighbor cells, however the model permits to prescribe this location for increased versatility. The typical stationary dome shaped interface between the liquid metal and electrolyte is shown in Figure 2 for the case of 500 kA cell. The interface shape can change in time if the cell is close to the stability limit due to the waves. For a stable cell the time average deformation of the aluminium-bath interface causes redistribution of the electric current, which accelerates consumption of the anode bottom in areas where the anode-cathode distance (ACD) is reduced. The time average shape of the anode bottom will eventually assume a shape similar to the stationary metal interface in order to preserve a constant ACD. The electric current in the liquid metal has large horizontal component due to the high electrical conductivity existing in regions close to the cell side where the bottom ledge starts. The shape of the cathode in the form of protrusions or depressions could affect the horizontal current density and redistribution. These three dimensional features of the electric current flow can be efficiently modeled using the relatively small depth to horizontal dimension ratio expansion model [5]. According to this model the general equations governing the DC current (which can change in time with the waves and anode burnout process) for the electric potential are:

$$\mathbf{j} = -\sigma \nabla \varphi, \tag{1}$$

$$\nabla^2 \varphi = 0 \tag{2}$$

The boundary conditions are the zero current at the insulating walls and the coupled current distribution $\mathbf{j}_a(x,y,t)$ at the anodes, $\mathbf{j}_c(x,y,t)$ at the cathode bottom. The distribution of $\mathbf{j}_a$ and $\mathbf{j}_c$ are obtained from the linear element resistivity network solution, which in turn is coupled to the computed potential distribution from the equation (2). At the interface between the liquid metal and the electrolyte the continuity of the potential and the normal component of electric current must be satisfied.

Since the depths of the liquid layers are extremely small if compared to their horizontal extension, the shallow layer approximation is an accurate and efficient way to solve this 3-dimensional problem. The solution in the aluminium layer can be obtained from the following equation:

$$j_{za}(x,y,t) - j_{zc}(x,y,t) = \sigma_{Al}\partial_k((H(x,y,t) - H_b(x,y))\partial_k\varphi), \tag{3}$$

where the aluminium interface H(x,y,t) and the bottom H_b(x,y) are variable. The current distribution at the top and the bottom depend on the iterative solution from the linear element resolution of the bus bars, anodes, pins, collector bars, etc. in the full network as shown in Figure 1.

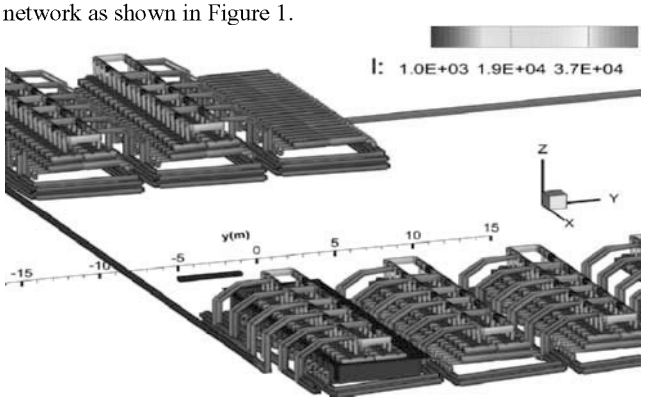

Figure 1. 500 kA cell in a potline at arbitrary position, showing the exit cell with prescribed connections to neighbour cells.

The magnetic field is created by the currents in the cell itself and from the complex bus-bar arrangement around the cell, in the neighbor cells, the return line and by the effect of construction steel magnetization. The full MHD model needs to account for the time-dependent coupling of the current and magnetic fields with the bath-metal interface movement. The magnetic field from the currents in the full bus-bar network is recalculated at each time step during the dynamic simulation using the Biot-Savart law. A very similar technique is used on the 3D grid within the cell fluid layers where an analytical technique is required to deal with the singularity in the Biot-Savart law to obtain the smooth solution.

3. The depth sensitive shallow layer model for hydrodynamics

The presence of open channels between the anodes and the gas filled grooves at the bottom of anodes is affecting the pressure distribution in the bulk of the electrolyte layer, particularly near the variable interface between the liquid metal and the electrolyte. The shallow layer fluid flow theory can be extended for a variable layer depth assuming the layer deformation is small, except for the channels, which impose the dominant hydrostatic pressure in the electrolyte layer (the 'connected vessels' principle). The vertical momentum equation for a small depth fluid reduces to quasi-hydrostatic equilibrium between the vertical pressure p variation and the gravity g:

$$0 = -\partial_z p - \rho g \,. \tag{4}$$

The pressure at any level z is

$$p(x, y, z) = p(H) + \rho g (H - z), \tag{5}$$

where the reference height $H(x,y,t)$ is the common interface between the liquid layers. The pressure at the top free surface of the electrolyte layer in the channels H_t, is constant, $p(H_t) = 0$. The surface H_t in the channels is practically flat and equal in all channels [1]. If the electrolyte channels (side, middle and between the individual anodes) are sufficiently deep, say 2-3 or more times the ACD, then this hydrostatic pressure will effectively act in all the electrolyte layer, similarly to the connected vessels principle. The electromagnetic force in the electrolyte will give very little modification to this dominant hydrostatic pressure. From (5) the pressure gradient variation at the electrolyte-metal interface $H(x,y,t)$ is

$$\begin{aligned} \partial_x p(H) &= -\rho_2 g \partial_x H \\ \partial_y p(H) &= -\rho_2 g \partial_y H. \end{aligned} \tag{6}$$

The approximation for the pressure and its horizontal gradient (6) at the unknown interface $H(x,y,t)$ are important for deriving the dynamic wave equation based on the momentum conservation and continuity in the two fluid layers in the electrolysis cell. After the depth averaging procedure is applied, the horizontal momentum equations in the two fluid layers (aluminium denoted by index i=1 and electrolyte - i=2) are:

$$\hat{\mathbf{u}} = (H_i - H)^{-1} \int \mathbf{u}\, dz \,, \tag{7}$$

$$\rho(\partial_t \hat{u}_j + \hat{u}_k \partial_k \hat{u}_j) = -\partial_j p(H) - \partial_j H - \mu \hat{u}_j + \partial_k \nu_e \partial_k \hat{u}_j + \hat{f}_j \tag{8}$$

The summation convention is assumed over the repeating indexes k (1 or 2, respectively for x, y coordinates). The effective turbulent viscosity $\nu_e(x,y,t)$ is computed according to the depth averaged version of k-ω two-equation turbulence model [5]. The equations (8) are used in the MHD model to determine directly the horizontal circulation velocity distribution.

The mathematical solution of the wave problem for the common interface $H(x,y,t)$ can be obtained by combining horizontal divergence of (8) and time derivative of the depth averaged continuity equation

$$\partial_t H = \partial_j [(H_i - H)\hat{u}_j] \,. \tag{9}$$

Taking into account the hydrostatic pressure gradient distribution (6) in the presence of the electrolyte channels, the non-linear wave equation for the aluminium-electrolyte interface $H(x,y,t)$ with the variable bottom H_1=H_b(x,y) and the top H_2 =$H_t(x,y)$ is

$$\left(\frac{\rho_1}{H - H_b} + \frac{\rho_2}{H_t - H}\right)\partial_{tt} H + \left(\frac{\rho_1 \mu_1}{H - H_b} + \frac{\rho_2 \mu_2}{H_t - H}\right)\partial_t H - (\rho_1 - \rho_2) g \partial_{jj} H = \tag{10}$$

$$\partial_j(-\hat{f}_{j1}) - [\rho_1 \partial_j(\hat{u}_{k1} \partial_k \hat{u}_{j1}) - \rho_2 \partial_j(\hat{u}_{k2} \partial_k \hat{u}_{j2})].$$

The boundary conditions are derived from the zero normal velocity condition at the cell walls. The linear stability model can be recovered from (10) by excluding the nonlinear horizontal velocity term and assuming that the H_b and H_t are constant. The equation (10) differs from the previous version with the solid lid top condition by the absence of the horizontal electromagnetic force contribution in the electrolyte, cf. [5].

4. Results for 500 kA cell with channels and cathode protrusions

The electrolyte channel effect

The present model permits to investigate the effects of the variable bottom and top of the cell on the MHD stability. The most important new physical effects are the wave propagation in the variable depth fluid layer and the increase of the horizontal electric current in the parts of the liquid metal layer of reduced depth. Both effects can alter the MHD stability conditions. The most striking difference is the 'dome' shaped stationary interface deformation in the case with the electrolyte channels, as can be seen from the Figure 2 for the 500 kA cell. The 'dome' interface is the feature of the 'benchmark' solution [9] used to validate various MHD solutions for the electrolysis cell. The channel model is essential in order to obtain the correct matching to this solution.

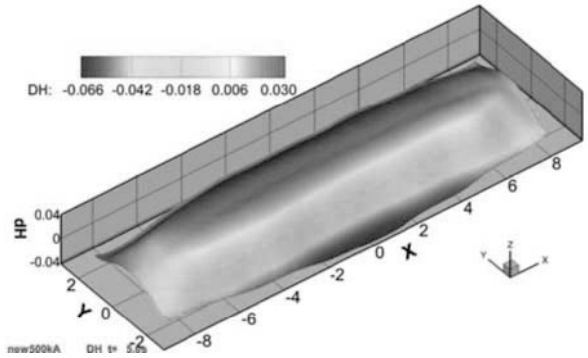

Figure 2. The interface deformation for 500 kA cell in a mid position of potline computed at stationary stage for I=500 kA, ACD=0.045 m, Hal=0.020 m, volume of liquid metal = 15.57 m^3

Apart from the 'stationary' interface deformation, the time-dependent evolution of the interface wave is changed in the presence of the open channels. Both cases are stable after the initial perturbation is slowly damped. Figure 3 demonstrates the differences in wave oscillation patterns. The high dome shaped interface is slightly slower in damping the oscillation of the excited frequency located between the 2nd and 3rd basic gravity wave modes. According to the theory [4], the unstable situation is characterized by a gradual shift of the interacting transversal

gravity wave frequencies until the original 2 independent oscillation frequencies coincide. The following resonant interaction gives rise to the rotating wave instability. In a realistic cell model as presented here, the frequency shift is clearly visible in Figure 3 for both cases of the channel model. However, without the channels (rigid anode condition at the top of electrolyte) the excited frequency is located at a larger frequency gravity wave range with high effective dissipation rate. In the case of the high 'dome' shaped interface, with the open channels, the dominant frequency appears at a lower value, indicating the interaction between the longitudinal (2,0) and the transversal (1,1) gravity wave modes. However, the presence of the turbulent dissipation is sufficient in this case to damp out the perturbation eventually.

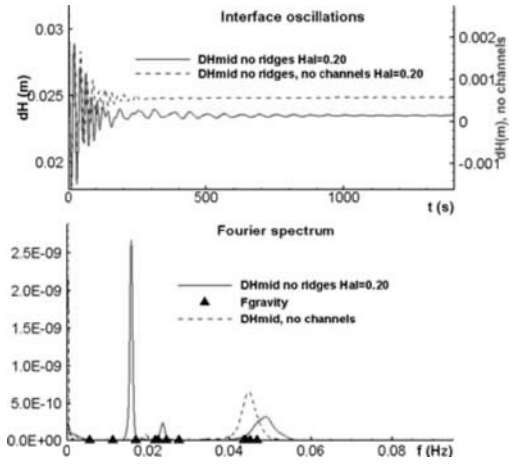

Figure 3. MHD stability by direct numerical simulation (at ACD=0.045 m, H_{Al}=0.020 m, volume of liquid Al = 15.57 m^3): comparison for the anode channel effects in the flat cathode bottom case

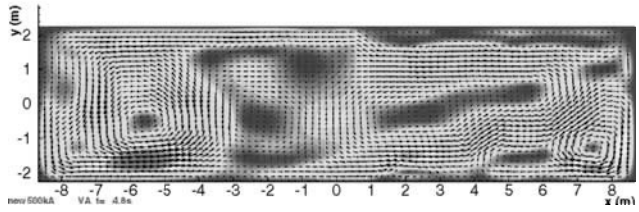

Figure 4. The horizontal velocity field in the flat cathode bottom case, V_{Al_max}=0.136 m/s.

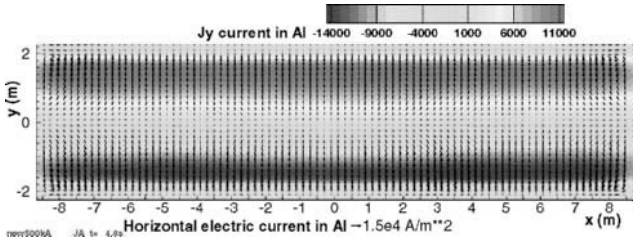

Figure 5. The electric current in liquid aluminium for the flat cathode bottom case, J_{yAl_max}=14000 A/m^2.

The horizontal circulation velocity field largely responsible for the turbulent dissipation is presented in Figure 4 for this case. The source for the horizontal velocity is the electromagnetic force which is directly proportional to the electric current distribution in the liquid aluminium shown in Figure 5.

The cathode protrusion effect

According to recent publications [6-8] a significant improvement to cell stability can be gained by introducing cathode design elements as local protrusions of various shapes. The reason is thought to be an increased damping of the horizontal velocities and the waves associated with these. Apparently the final result is sensitive to the overall cell design and the particular level of the magnetic field optimization. Nevertheless, we attempted to analyze the effect of the cathode elevation elements for the test 500 kA cell where the detailed busbar configuration is available in the open literature.

The first test case uses the cathode perturbations of 10 cm height arranged as shown in Figure 6. If the electric current is switched off, there can be a gravity wave excited after prescribing a perturbation of a particular mode as the initial condition. Figure 7 demonstrates the effect of the bottom ridges shown in Figure 6 on the pure gravity wave sloshing mode (1,0) by direct numerical simulation for the same 500 kA cell when I=0. The presence of ridges slightly reduces the observed frequency of the sloshing gravity wave and reduces the wave amplitude as the result of increased apparent damping. The shallow layer model reproduces the effect for the variable bottom case as expected.

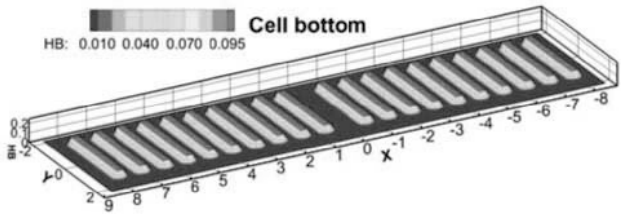

Figure 6. Bottom with 20 ridges, 10 cm high. (ACD=0.045 m, H_{Al}=0.020 m)

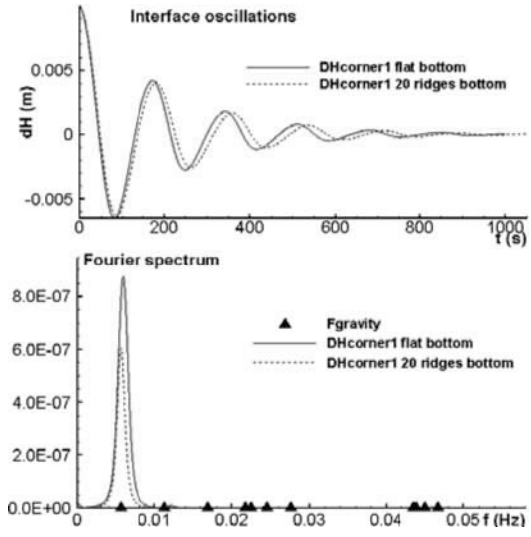

Figure 7. Effect of the bottom ridges on the pure gravity wave sloshing mode (1,0): ACD=0.045 m, H_{Al}=0.020 m, 10 cm ridges.

When the electric current I=500 kA is switched on the cell with the cathode ridges, as in Figure 6, has the horizontal circulation velocity field as shown in Figure 8 for the converged quasi-stationary state. If compared to the velocity in the reference case without the cathode ridges, the velocity magnitudes have unexpectedly increased. The explanation for this lies with the rise of the horizontal electric current density when the protruding ridges restrain the current in a smaller depth layer if the initial metal height is preserved as 20 cm above the lowest point of the cell bottom. The increase of the horizontal current is somewhat similar to the findings in [8]. The electric conductivity of the liquid metal is still considerably larger than the conductivity of cathode collector bar (iron). The small increase of the carbon resistivity for the ridge above the iron produces just a small variation along the x-axis of the exit current, as can be seen from Figure 9. The most important for the cell MHD stability is the magnitude of the horizontal current in the aluminium, as proven by the analytic solutions in [3,4]. The initial interface shape (Figure 10) looks rather similar to the case without the ridges (Figure 2), with a small decrease in the deformation magnitudes and noticeable indentations above the ridges beneath the metal layer.

The stability of the cell, however, suffers after the longer development of the interface waves. In about 200 s the wave amplitudes start to grow, reaching the stability limit at about 360 s when the waves crest short circuits to the anode (Figure 11). The presence of the 10 cm ridges, while conserving the metal height above the lowest bottom position, leads to a significant decrease of the metal volume in the cell (12.24 m^3 vs. 15.57 m^3 without ridges). This explains the rise of the horizontal current density and eventually the loss of MHD stability. If the volume of the liquid metal is increased by raising the level to 0.30 m, the cell regains stability according to the results in Figure 11. For a smaller size of the ridges 0.05 cm the stability is conserved for the metal level increase to 0.225 m.

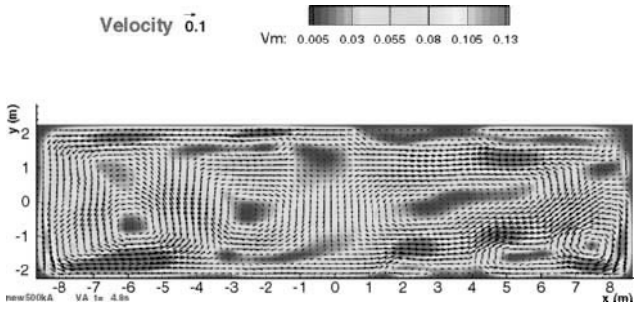

Figure 8. The horizontal velocity field for the 10 cm high ridges cathode bottom case, V_{Al_max}=0.165 m/s.

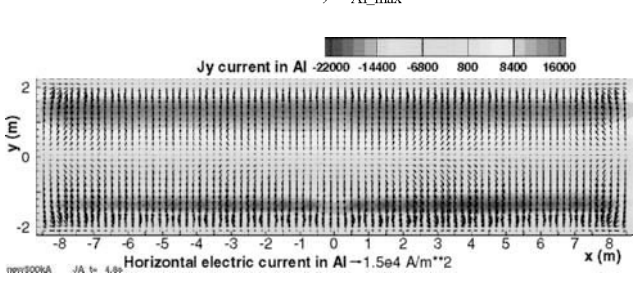

Figure 9. The electric current in liquid aluminium for the 10 cm high ridges cathode bottom case, J_{yAl_max}=22000 A/m^2.

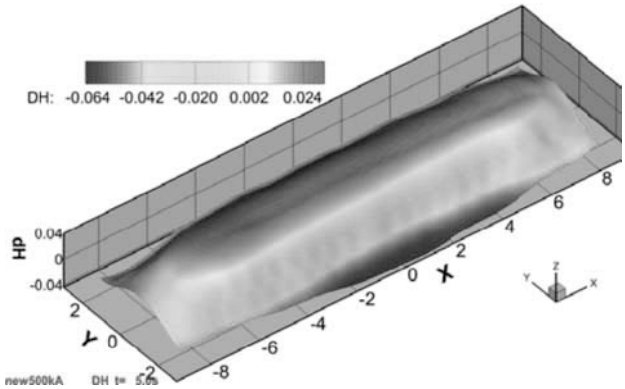

Figure 10. The interface deformation for 500 kA cell in a mid position of potline at the initial stage for the 10 cm high ridges cathode bottom case, volume of liquid metal = 12.24 m^3.

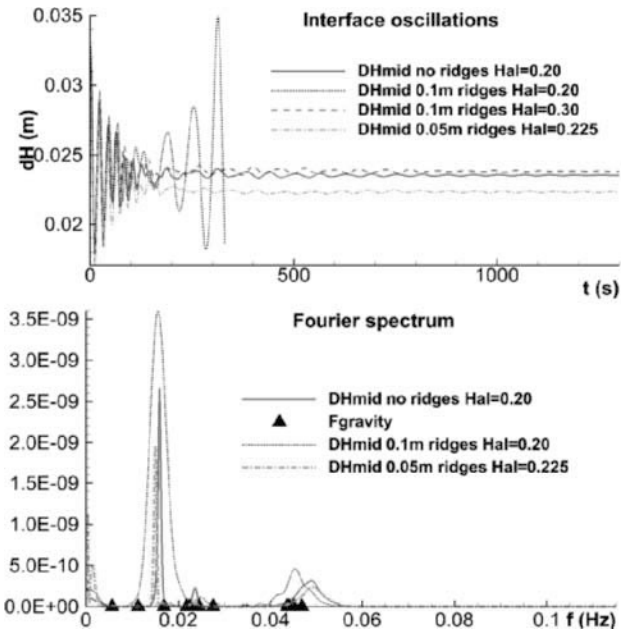

Figure 11. MHD stability by direct numerical simulation (at ACD=0.045 m, H_{Al} variable, variation of ridges shown in the Figure 6.

Very similar results were obtained by varying the shape of the bottom roughness elements, for instance, those shown in Figure 12: (1) ridges along the whole width of the cell, (2) cell with elevated side ledge and the ridges, (3) a cell with elongated depressions in the carbon cathode above the collector bars. All these types of the cathode were found to be unstable if the metal level is kept the same as in the flat cathode bottom case (0.20 m), however regaining the stability if the level of the metal is increased to preserve roughly the volume of the liquid metal in the cell.

The bottom ledge effect

Until now all the test cases considered the electrically non-conducting ledge at the cell bottom of a uniform width 0.20 m along the cell outer perimeter. The effect on the electric current is

clearly visible in Figures 5 and 9. The presence of the cathode ridges can affect the ledge formation at the cathode bottom by promoting the sediment collection in the lower parts between the cathode elevations. Alternatively the thermal transfer could be affected in the presence of the thicker cathode, equally affecting the ledge formation. Numerical experiments with the MHD program permit to investigate these options. The particular ledge shape tested is shown in Figure 13, however the program permits inputs to create various combinations by the user. In this case the insulated bottom along the side perimeter penetrates to 40 cm inwards in the locations between the 5 cm high ridges, while staying 20 cm on the top of the elevated ridges. The metal depth was adjusted to 0.225 m in order to preserve the liquid metal volume (15.77 m^3) at the value close to the reference case (15.57 m^3). The case was found to be beneficial for cell stability, as shown by the dash-dotted line in Figure 11. The horizontal velocity was reduced in comparison to the flat bottom reference case (compare Figures 14 and 4) with the maximum velocity magnitude down to 0.123 m/s from 0.136 m/s. The stationary interface deformation is reduced as well for the variable ledge and 5 cm ridges case as can be seen comparing the shapes in Figures 2 and 15. The effect of the electric currents due to the variable ledge can be felt along the interface edges as a wavy shape, which is not affecting the overall stability of the cell or could be even beneficial in the damping process of the larger scale rotating waves.

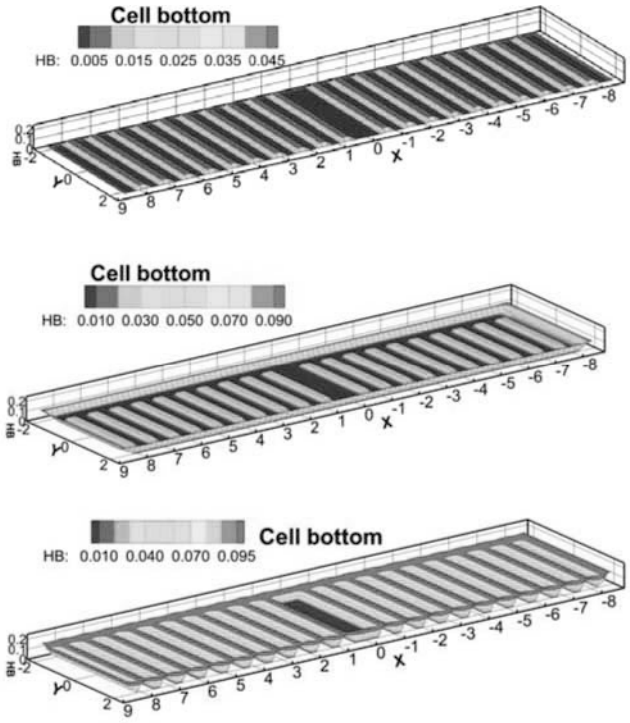

Figure 12. Various tested cathode bottom shapes with ridges or depressions and elevated ledge shape.

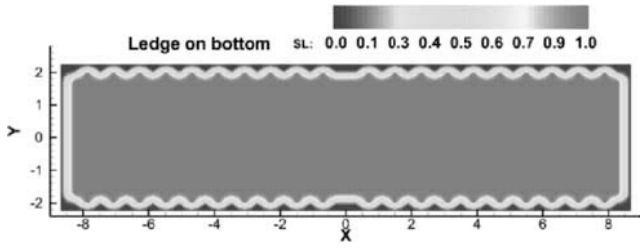

Figure 13. Variable ledge along side walls, insulated bottom between ridges

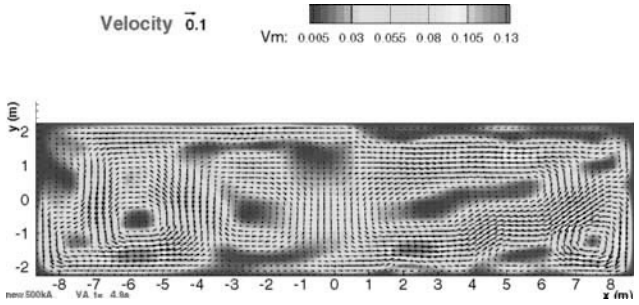

Figure 14. The horizontal velocity field for the 5 cm high ridges cathode bottom and the variable ledge case, V_{Al_max}=0.123 m/s.

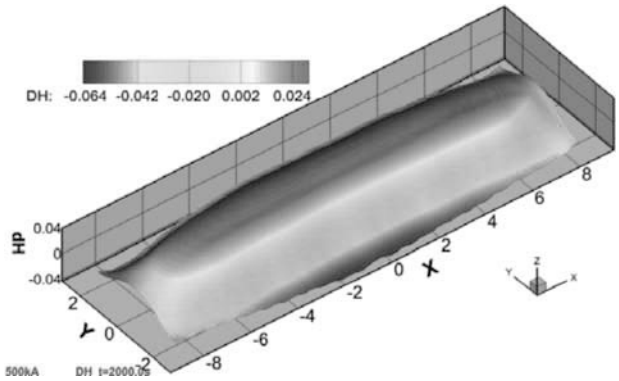

Figure 15. The interface deformation for 500 kA cell in a mid position of potline at the final stage after 2000 s for the 5 cm high ridges cathode bottom and the variable ledge case, volume of liquid metal = 15.77 m^3.

Conclusions

The MHD model for the non-linear cell stability analysis software was updated to account for the deformed bottom and top surfaces of the cell cavity. The non-linear cell stability analysis results show that the presence of open electrolyte channels is affecting the cell stability.

The effect of bottom friction enhancing elements is evaluated using the depth sensitive turbulent velocity model. The sloshing gravity wave without MHD interaction is confirmed to be damped moderately in the presence of the bottom ridge elements. The MHD interaction is strongly affected by the increase in the horizontal electric current density on top of the ridge elements. There is a danger to create MHD instability if the bottom ridge

elements are added without optimization. When the volume of liquid metal is increased in proportion to the volume occupied by the bottom ridges, the MHD stability is preserved as in the reference case. The non-uniform insulating ledge position in association with the bottom elevation elements requires coupled analysis of thermal, electrical and momentum transport in the reduction cells.

References

1. R. Moreau and J.W. Evans. An analysis of the hydrodynamics of aluminium reduction cells. *Journal of Electrochemical Society*, 131 (1984), no. 10, pp. 2251-2259.
2. V. Bojarevics and K. Pericleous, Solutions for the Metal-Bath Interface in Aluminium Electrolysis Cells. *In Proceedings of TMS Light Metals* (2009), pp. 569-574.
3. Urata, N., Mori, K. and Ikeuchi, H. Behavior of bath and molten metal in aluminium electrolytic cell. *Keikinzoku*, 26 (1976), no. 11, pp. 573-600.
4. V. Bojarevics and M. V. Romerio. Long waves instability of liquid metal-electrolyte interface in aluminium electrolysis cells: a generalization of Sele's criterion. *Eur. J. Mech., B/Fluids*, 13 (1994), no 1, pp. 33-56.
5. V. Bojarevics and K. Pericleous. Shallow Water Model for Aluminium Electrolysis Cells with Variable Top and Bottom. *In Proceedings of TMS Light Metals* (2008), pp. 403-408.
6. N.X.Feng, Y.F.Tian, J.P.Peng, et al. New Cathodes in Aluminum Reduction Cells, *In Proceedings of TMS Light Metals* (2010), pp. 405-408.
7. J.P. Peng, N.X.Feng, S.F. Feng, J.Liu, X.Q. Qi : "Development and Application of an Energy Saving Technology for Aluminium Reduction cells", *In Proceedings of TMS Light Metals* (2011), pp. 1023-1027.
8. B. Li, F. Wang, X. Zhang, F. Qi, N. Feng. Development and Application of an Energy Saving Technology for Aluminium Reduction cells. *In Proceedings of TMS Light Metals* (2012), pp. 865-868.
9. D.S. Severo, V. Gusberti, A.F. Schneider, E.C. Pinto and V. Potocnik, "Comparison of Various Methods for Modeling the Metal-Bath Interface". *In Proceedings of TMS Light Metals* (2008), pp. 413-418.